



# Recent Additions in the Modeling Capabilities of an Open-Source Wave Energy Converter Design Tool

## Preprint

N. Tom, M. Lawson, and Y.-H. Yu  
*National Renewable Energy Laboratory*

*To be presented at the International Offshore and Polar Engineering Conference (ISOPE 2015)  
Kona, Hawaii  
June 21–26, 2015*

**NREL is a national laboratory of the U.S. Department of Energy  
Office of Energy Efficiency & Renewable Energy  
Operated by the Alliance for Sustainable Energy, LLC**

This report is available at no cost from the National Renewable Energy Laboratory (NREL) at [www.nrel.gov/publications](http://www.nrel.gov/publications).

**Conference Paper**  
NREL/CP-5000-63905  
April 2015

Contract No. DE-AC36-08GO28308

## NOTICE

The submitted manuscript has been offered by an employee of the Alliance for Sustainable Energy, LLC (Alliance), a contractor of the US Government under Contract No. DE-AC36-08GO28308. Accordingly, the US Government and Alliance retain a nonexclusive royalty-free license to publish or reproduce the published form of this contribution, or allow others to do so, for US Government purposes.

This report was prepared as an account of work sponsored by an agency of the United States government. Neither the United States government nor any agency thereof, nor any of their employees, makes any warranty, express or implied, or assumes any legal liability or responsibility for the accuracy, completeness, or usefulness of any information, apparatus, product, or process disclosed, or represents that its use would not infringe privately owned rights. Reference herein to any specific commercial product, process, or service by trade name, trademark, manufacturer, or otherwise does not necessarily constitute or imply its endorsement, recommendation, or favoring by the United States government or any agency thereof. The views and opinions of authors expressed herein do not necessarily state or reflect those of the United States government or any agency thereof.

This report is available at no cost from the National Renewable Energy Laboratory (NREL) at [www.nrel.gov/publications](http://www.nrel.gov/publications).

Available electronically at SciTech Connect <http://www.osti.gov/scitech>

Available for a processing fee to U.S. Department of Energy and its contractors, in paper, from:

U.S. Department of Energy  
Office of Scientific and Technical Information  
P.O. Box 62  
Oak Ridge, TN 37831-0062  
OSTI <http://www.osti.gov>  
Phone: 865.576.8401  
Fax: 865.576.5728  
Email: [reports@osti.gov](mailto:reports@osti.gov)

Available for sale to the public, in paper, from:

U.S. Department of Commerce  
National Technical Information Service  
5301 Shawnee Road  
Alexandria, VA 22312  
NTIS <http://www.ntis.gov>  
Phone: 800.553.6847 or 703.605.6000  
Fax: 703.605.6900  
Email: [orders@ntis.gov](mailto:orders@ntis.gov)

*Cover Photos by Dennis Schroeder: (left to right) NREL 26173, NREL 18302, NREL 19758, NREL 29642, NREL 19795.*

NREL prints on paper that contains recycled content.

# Recent Additions in the Modeling Capabilities of an Open-Source Wave Energy Converter Design Tool

*Nathan Tom, Michael Lawson, Yi-Hsiang Yu*

National Wind Technology Center, National Renewable Energy Laboratory.  
Golden, Colorado, USA

## ABSTRACT

WEC-Sim is a midfidelity numerical tool for modeling wave energy conversion devices. The tool's code employs the MATLAB SimMechanics package to solve multibody dynamics and model wave interactions using hydrodynamic coefficients derived from frequency-domain boundary-element methods. This paper presents the new modeling features introduced in the latest release of WEC-Sim. The first feature is conversion of the fluid memory kernel to a state-space form. This enhancement offers a substantial computational benefit after the hydrodynamic body-to-body coefficients are introduced and the number of interactions increases exponentially with each additional body. Additional features include the ability to calculate the wave-excitation forces based on the instantaneous incident wave angle, allowing the device to weathervane, as well as import a user-defined wave elevation time series. A review of the hydrodynamic theory for each feature is provided and the successful implementation is verified using test cases.

**KEY WORDS:** Wave energy converter; open source; modeling software; WEC-Sim; NREL.

## INTRODUCTION

During the past decade, there has been a renewed interest from both the commercial and governmental sectors in the development of marine and hydrokinetic (MHK) energy; however, wave energy converters (WECs) are still in the early stages of development and have not yet been proven to be commercially viable. Given the relatively few full-scale WEC device deployments that currently exist, development heavily depends on numerical modeling tools to drive innovative designs and advanced control strategies. Conventional seakeeping software has a difficult time modeling new multibody WECs. These complications arise because of the various links between bodies and the additional degrees of freedom required to model the power extraction process.

WEC modeling tools are now being developed by several companies; these include WaveDyn, distributed by Det Norske Veritas – Germanischer Lloyd (DNV GL) (Mackay, Cruz, Livingstone, and Arnold, 2013); OrcaFlex, distributed by Orcina (Orcina, 2014); Aqwa,

distributed by ANSYS; and INWAVE, distributed by INNOSEA (Combourieu, Maxime, Francois, and Barbarit, 2014). Still, it is desirable to develop open-source modeling tools to establish a collaborative research community that can play a role in accelerating the pace of MHK technology development in the United States. To assist in this effort, the U.S. Department of Energy (LaBonte et al., 2013) funded a joint initiative between the National Renewable Energy Laboratory (NREL) and Sandia National Laboratories (SNL) to develop a comprehensive wave energy modeling tool. This joint effort led to the release of WEC-Sim-v1.0 (Yu, Lawson, Ruehl, Michelen, and Tom, 2014) in the summer of 2014. The code was developed in the MATLAB/SIMULINK (MATLAB, 2014) environment using the multibody dynamics solver SimMechanics with preliminary code verification provided in Ruehl, Michelen, Kanner, Lawson, and Yu, 2014; Yu, Li, Hallet, and Hotimsky, 2014. Today, WEC-Sim is best suited to handle rigid multibody dynamics that allow for multiple linkages; however, overtopping and oscillating water column WEC concepts cannot be easily modeled at this time.

This paper provides an overview of the additional modeling capabilities included in WEC-Sim-v1.1 released in March 2015. The first module described in this paper is the conversion of the fluid memory kernel to state-space form. This ability will help reduce computational time once the module for hydrodynamic body-to-body interactions is introduced. The final hydrodynamic modules include the weathervaning capability, which uses wave-excitation forces calculated from the instantaneous incident wave angle, and importation of a user-defined wave elevation time series. The hydrodynamic theory for each feature is provided as well as the results from test cases that were used to verify the successful implementation of these features within WEC-Sim.

## STATE-SPACE REPRESENTATION OF THE IMPULSE RESPONSE FUNCTION

In linear water wave theory, the instantaneous wave radiation force, commonly known as the Cummins equation (Cummins, 1962), can be written as:

$$f_r(t) = -\mu_\infty \ddot{\zeta}(t) - \lambda_\infty \dot{\zeta}(t) - \int_{-\infty}^t K_r(t-\tau) \dot{\zeta}(\tau) d\tau \quad (1)$$

where  $\mu_\infty$  is the added mass at infinite frequency,  $\lambda_\infty$  is the wave damping at infinite frequency,  $K_r$  is a causal function known as the radiation impulse-response function, and  $\zeta$  is the six-degrees-of-freedom vector of body motion. The convolution term in Eq. (1) captures the effect that the changes in momentum of the fluid at a particular time affect the motion at future instances, which can be thought of as a fluid memory effect. The relations between the time- and frequency-domain coefficients were derived in Ogilve (1964) as follows:

$$\lambda(\sigma) = \lambda_\infty + \int_0^\infty K_r(t) \cos \sigma t dt \quad (2)$$

$$\mu(\sigma) = \mu_\infty - \frac{1}{\sigma} \int_0^\infty K_r(t) \sin \sigma t dt \quad (3)$$

where  $\mu(\sigma)$  and  $\lambda(\sigma)$  are the frequency-dependent hydrodynamic radiation coefficients commonly known as the added mass and wave-damping. The  $\infty$  subscripts denote the added mass and wave-damping values at infinite frequency.

The radiation impulse response function can be calculated by taking the inverse Fourier transform of the hydrodynamic radiation coefficients, as found by:

$$K_r(t) = -\frac{2}{\pi} \int_0^\infty \sigma [\mu(\sigma) - \mu_\infty] \sin \sigma t d\sigma \quad (4)$$

$$K_r(t) = \frac{2}{\pi} \int_0^\infty [\lambda(\sigma) - \lambda_\infty] \cos \sigma t d\sigma \quad (5)$$

where the frequency response of the convolution will be given by:

$$\begin{aligned} K_r(j\sigma) &= \int_0^\infty K_r(t) e^{-j\sigma t} dt \\ &= [\lambda(\sigma) - \lambda_\infty] + j\sigma [\mu(\sigma) - \mu_\infty] \end{aligned} \quad (6)$$

and  $j$  is the imaginary unit  $\sqrt{-1}$ . For most single floating bodies  $\lambda_\infty = 0$  and Eq. (5) converges significantly faster than Eq. (4). The hydrodynamic coefficients are solely a function of geometry and the frequency-dependent added mass and wave-damping values can be obtained from boundary element solvers such as WAMIT (Lee, 1995) and NEMOH (Barbarit, 2014).

It is highly desirable to represent the convolution integral of Eq. (1) in state-space form (Yu and Falnes, 1996). This has been shown to dramatically increase computational speeds and allow for use of conventional control methods, which rely on linear state-space models. An approximation will need to be made because  $K_r$  is obtained from a set of partial differential equations whereas a linear state-space model is constructed from a set of ordinary differential equations. In general it is desired to make the following approximation:

$$\begin{aligned} \dot{X}_r(t) &= A_r X_r(t) + B_r \dot{\zeta}(t); \quad X_r(0) = 0 \\ \int_{-\infty}^t K_r(t-\tau) d\tau &\approx C_r X_r(t) + D_r \dot{\zeta}(t) \end{aligned} \quad (7)$$

where  $A_r$ ,  $B_r$ ,  $C_r$ ,  $D_r$  are the time-invariant state, input, output, and feed-through matrices;  $X_r$  is the vector of states that describe the convolution

kernel as time progresses; and  $\dot{\zeta}$  is the body velocity. The impulse-response of a single-input state-space model represented by:

$$\begin{aligned} \dot{x}(t) &= A_r x(t) + B_r u(t) \\ y(t) &= C_r x(t) \end{aligned} \quad (8)$$

is the same as the unforced response ( $u = 0$ ) with the initial states set to  $B_r$ . The impulse response of a continuous system with a nonzero  $D_r$  matrix is infinite at  $t = 0$ , therefore the lower continuity value of  $C_r B_r$  is reported at  $t = 0$ ; however, if a  $D_r$  matrix results from a given realization method it can be artificially set to 0 with minimal effect on the system response. The general solution to a linear-time invariant system can be calculated from:

$$x(t) = e^{A_r t} x(0) + \int_0^t e^{A_r(t-\tau)} B_r u(\tau) d\tau \quad (9)$$

where  $e^{A_r t}$  is called the matrix exponential and the calculation of  $K_r$  follows:

$$\tilde{K}_r(t) = C_r e^{A_r t} B_r. \quad (10)$$

## Laplace Transform and Transfer Function

The Laplace transform is a common integral transform in mathematics. It is a linear operator of a function that transforms  $f(t)$  to a function  $F(s)$  with complex argument,  $s$ , which is obtained from:

$$F(s) = \int_0^\infty f(t) e^{-st} dt \quad (11)$$

where the derivative of  $f(t)$  has the following Laplace transform:

$$sF(s) = \int_0^\infty \frac{df(t)}{dt} e^{-st} dt \quad (12)$$

Consider a linear input-output system described by the following differential equation:

$$\begin{aligned} \frac{d^m y}{dt^m} + a_1 \frac{d^{m-1} y}{dt^{m-1}} + \dots + a_m y \\ = b_0 \frac{d^n u}{dt^n} + b_1 \frac{d^{n-1} u}{dt^{n-1}} + \dots + b_n u \end{aligned} \quad (13)$$

where  $y$  is the output and  $u$  the input. After taking the Laplace transform of Eq. (13), the differential equation is now described by two polynomials:

$$\begin{aligned} A(s) &= s^m + a_1 s^{m-1} + \dots + a_{m-1} s + a_m \\ B(s) &= b_0 s^n + b_1 s^{n-1} + \dots + b_{n-1} s + b_n \end{aligned} \quad (14)$$

where  $A(s)$  is the characteristic polynomial of the system. The polynomials can be inserted into Eq. (13) leading to:

$$G(s) = \frac{Y(s)}{U(s)} = \frac{s^m + a_1 s^{m-1} + \dots + a_{m-1} s + a_m}{b_0 s^n + b_1 s^{n-1} + \dots + b_{n-1} s + b_n} \quad (15)$$

where  $G(s)$  is the transfer function. If the state input, output, and feed-through matrices are known, the transfer function of the system can be calculated from:

$$G(s) = C_r(sI - A_r)^{-1}B_r + D_r. \quad (16)$$

The frequency response of the system can be obtained by substituting  $j\sigma$  for  $s$ , over the frequency range of interest, where the magnitude and phase of  $G(j\sigma)$  can be calculated with results commonly presented in a Bode plot.

### Realization Theory – Frequency Domain

Currently, WEC-Sim allows for the state-space realization of the hydrodynamic radiation coefficients either in the frequency domain (FD) or time domain (TD); however, the frequency-domain realization requires the Signal Processing Toolbox distributed by MATLAB. In this analysis the frequency response,  $K_r(j\sigma)$ , of the impulse-response function is used to best fit a rational transfer function  $G(s)$ , which is then converted to a state-space model. The general form of a single-input, single-output transfer function of order  $n$  and relative degree  $n-m$  is given by:

$$G(s, \gamma) = \frac{A(s, \gamma)}{B(s, \gamma)} = \frac{s^m + a_1s^{m-1} + \dots + a_m}{b_0s^n + b_1s^{n-1} + \dots + b_n} \quad (17)$$

$$\gamma = [a_1, \dots, a_m, b_0, \dots, b_n]^T. \quad (18)$$

WEC-Sim utilizes a nonlinear least-squares solver to estimate the parameters of  $\gamma$ . The estimation can only be made after the order and relative degree of  $G(s)$  are decided, at which point the following least-squares minimization can be performed:

$$\gamma^* = \arg \min_{\gamma} \sum_i w_i \left| K_r(j\sigma) - \frac{A(j\sigma)}{B(j\sigma)} \right|^2 \quad (19)$$

where  $w_i$  is an individual weighting value for each frequency. An alternative that linearizes Eq. (19), proposed by Taghipour, Perez, and Moan (2008), which requires the weights to be chosen as:

$$w_i = |B(j\sigma, \gamma)|^2 \quad (20)$$

which reduces the problem to:

$$\gamma^* = \arg \min_{\gamma} \sum_i |B(j\sigma, \gamma)K_r(j\sigma) - A(j\sigma, \gamma)|^2. \quad (21)$$

Even so, depending on the data to be fitted, the transfer function may be unstable, because stability is not a constraint used in the minimization. If this occurs, the unstable poles are reflected about the imaginary axis. The relative order of the transfer function can be determined from the initial value theorem:

$$\lim_{t \rightarrow 0} K_r(t) = \lim_{s \rightarrow \infty} sK_r(s) = \lim_{s \rightarrow \infty} s \frac{A(s)}{B(s)} = \frac{s^{m+1}}{b_0s^n}. \quad (22)$$

For this limit to be finite and nonzero the relative order of the transfer function must be one ( $n = m + 1$ ).

### Realization Theory – Time Domain

This methodology consists of finding the minimal order of the system and the discrete time state matrices ( $A_d, B_d, C_d, D_d$ ) from samples of the impulse-response function. This problem is easier to handle for a discrete-time system, because the impulse-response function is given by the Markov parameters of the system:

$$\tilde{K}_r(t_k) = C_d A_d^k B_d \quad (23)$$

where  $t_k = k\Delta t$  for  $k = 0, 1, 2, \dots$  and  $\Delta t$  is the sampling period. The previous equation does not include the feed-through matrix because it results in an infinite value at  $t=0$  and is removed to keep the causality of the system.

The most common algorithm to obtain the realization is to perform a singular value decomposition (SVD) on the Hankel matrix of the impulse-response function as proposed in Kung (1978). The order of the system and corresponding state-space parameters are determined from the number of significant Hankel singular values. Performing an SVD produces:

$$H = \begin{bmatrix} K_r(2) & K_r(3) & \dots & K_r(n) \\ K_r(3) & K_r(4) & \dots & 0 \\ \vdots & \vdots & \ddots & \vdots \\ K_r(n) & 0 & \dots & 0 \end{bmatrix} \quad (24)$$

$$H = U\Sigma V^* \quad (25)$$

where  $H$  is the Hankel matrix, and  $\Sigma$  is a diagonal matrix containing the Hankel singular values in descending order. Examination of the Hankel singular values reveals there are generally only a small number of significant states, and model reduction can be performed without a significant loss in accuracy (Taghipour, Perez, and Moan, 2008; Kristiansen, Hijulstad, and Egeland, 2005). Further detail about the SVD method and calculation of the state-space parameters will not be discussed in this paper, and the reader is referred to Kung, 1978; Taghipour, Perez, and Moan, 2008; and Kristiansen, Hijulstad, and Egeland, 2005.

### Quality of Realization

WEC-Sim evaluates the quality of the resulting state-space model via the frequency response when using the frequency-domain realization and the corresponding impulse-response for the time-domain realization. To evaluate these responses the coefficient of determination,  $R^2$ , is computed according to:

$$R^2 = 1 - \frac{\sum (K_r - \tilde{K}_r)^2}{\sum (K_r - \bar{K}_r)^2} \quad (26)$$

where  $\tilde{K}_r$  represents the resulting hydrodynamic values from the state-space model and  $\bar{K}_r$  is the mean value of the reference (true) values. The summations are performed across all frequencies to provide a measure of the variability of the function that is captured by the model.

### Application of State-Space Realization

A truncated vertical cylindrical floater has been chosen as the sample geometry to compare the frequency- and time-domain realizations. The floater geometric parameters and tank dimensions are found in Table 1

and the hydrodynamic radiation coefficients were calculated from Yeung (1981). The hydrodynamic coefficients were obtained between 0.05 rad/s and -11 rad/s at 0.05 rad spacing.

In this example, an  $R^2$  threshold of 0.99 was set and the resulting realizations for the impulse-response function and the frequency-dependent radiation coefficients are found in Fig. 1 and Fig. 2. In this example the time-domain characterization outperforms the frequency-domain regression, and the major difference appears in the wave-damping estimation. It was found that the time-domain characterization had better stability than the frequency-domain regression, because it does not require reflection of the unstable poles about the imaginary axis. The results from WEC-Sim also had good agreement when compared to the MSS FDI Toolbox (Perez and Fossen, 2009) developed at the Norwegian University of Science and Technology. WEC-Sim users should check the quality of the hydrodynamic data with the custom WEC-Sim MATLAB functions that perform the realizations without running full simulations. These codes allow users to set fitting parameters using an iterative interface that plots how the fit changes with increasing state-space order.

Table 1. Floater geometric parameters and tank dimensions.

$D$ (diameter) = $2a$ = 0.273 m	$d$ (draft) = 0.613 m	$h$ (tank depth) = 1.46 m
------------------------------------	--------------------------	------------------------------

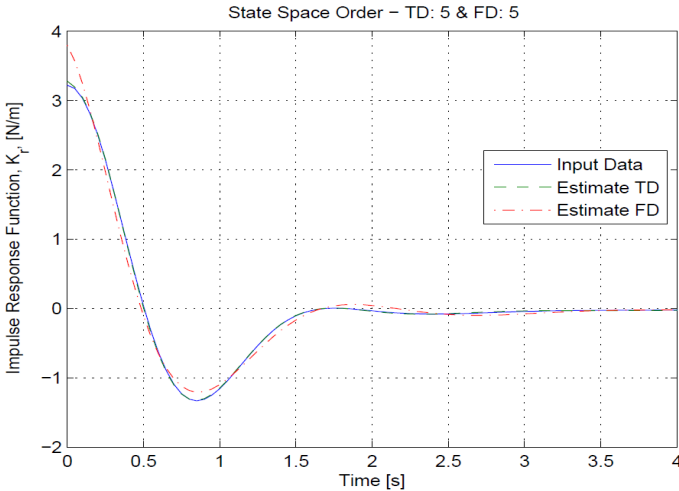


Fig. 1. Comparison of  $K_r$  to time- and frequency- domain realizations

#### HYDRODYNAMIC CROSS-COUPLING FORCES

For a single floating body, the time-domain representation of the radiation forces is given by Eq. 1, because it is dependent only on its own motion. However, most WECs consist of multiple floating bodies that can be in very close proximity, and as a result, additional interaction forces arise. These forces are generated as the motion of nearby floating bodies alters the local wave field. Unique to floating-body hydrodynamics are the forces felt by one body because of the motion of “n” additional bodies. This is reflected in the off diagonal terms of the added mass and wave-damping matrices which generate a force on Body 1 because of the acceleration and velocity of bodies 2 through n. Because of the reciprocity relationship (Newman, 1977), a consequence of applying Green’s Second Identity, the cross diagonal hydrodynamic coefficients are equal:

$$\mu_{ij} + \frac{\lambda_{ij}}{-j\sigma} = \mu_{ji} + \frac{\lambda_{ji}}{-j\sigma}. \quad (27)$$

Thus, a symmetry check can be performed on the numerical values obtained from boundary element solvers, such as WAMIT and NEMOH.

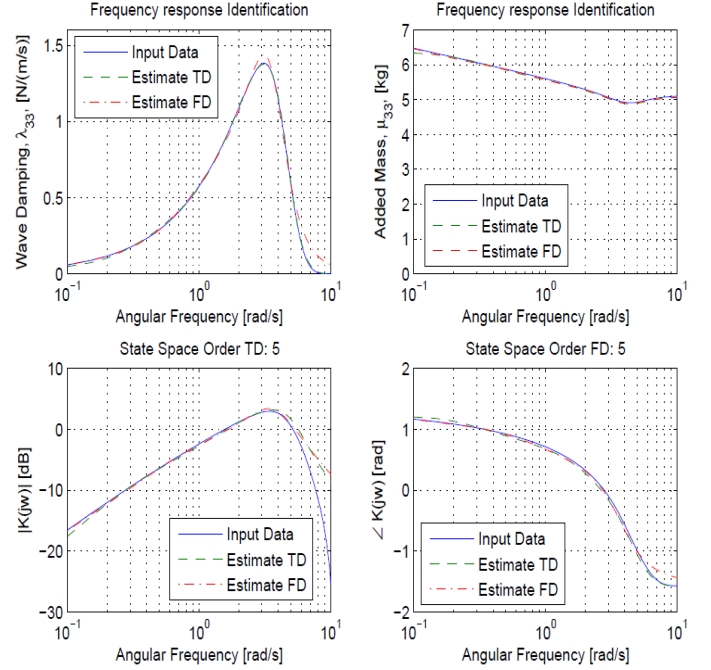


Fig. 2. Frequency response of time- and frequency-domain realizations

#### Response Amplitude Operator (RAO)

It is common practice to calculate the response amplitude operator to access the performance of a WEC. For an incident wave of amplitude  $A$  and frequency  $\sigma$ , the response of the floating body is given by  $\zeta_i$ :

$$\eta(x, t) = \Re \{ A e^{j(\sigma t - kx)} \} \quad (28)$$

$$\zeta_i(t) = \Re \{ \xi_i e^{j\sigma t} \} \quad (29)$$

where  $\eta$  is the surface elevation,  $k$  is the wave number and  $\xi_i$  is the complex amplitude of motion for the  $i$ -th direction. The resulting harmonic motion, when allowing six degrees of freedom for all floating bodies, can be described by the following coupled system of differential equations:

$$\sum_{k=1}^{6 \times n} [C_{ik} - \sigma^2(I_{ik} + M_{ik}) + j\sigma\Lambda_{ik}] \xi_k = F_i \quad (30)$$

where  $I_{ik}$  is the generalized inertia matrix for all floating bodies,  $\Lambda_{ik}$  is the generalized wave damping matrix,  $M_{ik}$  is the generalized added mass matrix,  $C_{ik}$  is the restoring matrix, and  $F_i$  is the complex amplitude of the wave-exciting force for all floating bodies. The full description of the matrices can be found in Newman (1977) or another introductory hydrodynamic textbook.

#### Validation of a Generic Five-Body WEC

A generic set of five identical point absorbers were chosen to validate WEC-Sim’s ability to handle multibody interactions. For demonstration purposes, all bodies will be constrained to heave, allowing one to simplify Eq. (30), though extending the equation of motion to consider additional degrees of freedom is easily achieved.

The Simulink model constructed for this task can be seen in Fig. 3.

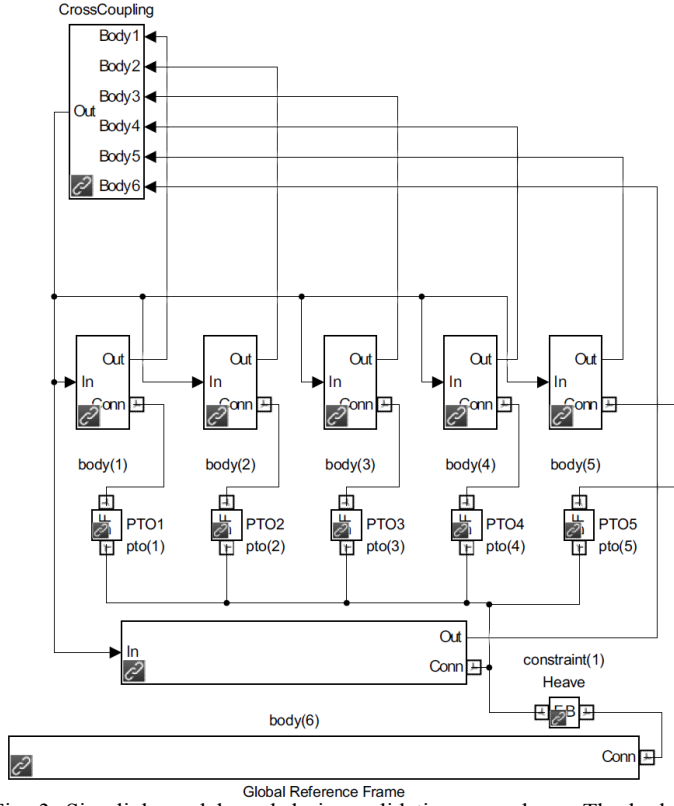


Fig. 3. Simulink model used during validation procedure. The body, constraint, PTO, and cross coupling blocks are custom built and appear in the Simulink library.

### Inclusion of Linear Power-Take-Off System

In order to extract any power from the incident waves a power-take-off (PTO) system is required, predominantly either a hydraulic or electrical generator. The generic form of the PTO reaction force is given by:

$$f_{PTO} = -C_g \dot{\zeta}_{rel} - B_g \ddot{\zeta}_{rel} - \mu_g \ddot{\zeta}_{rel} \quad (31)$$

where  $\zeta_{rel}$  is the relative motion between the floating bodies to which the PTO is attached. However, for this test case, each point absorber is attached to a fixed submerged body. Thus, the relative velocity will reduce to the velocity of each body. The generator spring, damping, and inertia force coefficients are given by  $C_g$ ,  $B_g$ , and  $\mu_g$ , respectively. In the frequency domain, adding the PTO force contribution to Eq. (30), while zeroing  $C_g$  and  $\mu_g$ , gives:

$$\begin{aligned} & \underbrace{\left[ C_{33} - \sigma^2(m_1 + \mu_{33}) \right] + j\sigma[\lambda_{33} + B_g]}_{a_1} \zeta_3 \\ & + \underbrace{\left[ -\sigma^2 \mu_{39} + j\sigma \lambda_{39} \right]}_{b_1} \zeta_9 + \underbrace{\left[ -\sigma^2 \mu_{315} + j\sigma \lambda_{315} \right]}_{c_1} \zeta_{15} \\ & + \underbrace{\left[ -\sigma^2 \mu_{321} + j\sigma \lambda_{321} \right]}_{d_1} \zeta_{21} + \underbrace{\left[ -\sigma^2 \mu_{327} + j\sigma \lambda_{327} \right]}_{e_1} \zeta_{27} = AX_3 \end{aligned} \quad (32)$$

$$\begin{aligned} & \underbrace{\left[ -\sigma^2 \mu_{93} + j\sigma \lambda_{93} \right]}_{a_2} \zeta_3 + \underbrace{\left[ C_{99} - \sigma^2(m_2 + \mu_{99}) \right] + j\sigma[\lambda_{99} + B_g]}_{b_2} \zeta_9 \\ & + \underbrace{\left[ -\sigma^2 \mu_{915} + j\sigma \lambda_{915} \right]}_{c_2} \zeta_{15} + \underbrace{\left[ -\sigma^2 \mu_{921} + j\sigma \lambda_{921} \right]}_{d_2} \zeta_{21} \\ & + \underbrace{\left[ -\sigma^2 \mu_{927} + j\sigma \lambda_{927} \right]}_{e_2} \zeta_{27} = AX_9 \end{aligned} \quad (33)$$

where  $X_i$  is the wave-exciting force per unit-wave-amplitude. Subscripts 3 and 9 denote the first two bodies and three additional equations are necessary to complete the entire system. The previous system of equations can be solved to obtain the complex amplitudes of motion ( $\zeta_3$ ,  $\zeta_9$ ,  $\zeta_{15}$ ,  $\zeta_{21}$ ,  $\zeta_{27}$ ) from basic matrix algebra:

$$\begin{bmatrix} \zeta_3 / A \\ \zeta_9 / A \\ \zeta_{15} / A \\ \zeta_{21} / A \\ \zeta_{27} / A \end{bmatrix} = \begin{bmatrix} a_1 & b_1 & c_1 & d_1 & e_1 \\ a_2 & b_2 & c_2 & d_2 & e_2 \\ a_3 & b_3 & c_3 & d_3 & e_3 \\ a_4 & b_4 & c_4 & d_4 & e_4 \\ a_5 & b_5 & c_5 & d_5 & e_5 \end{bmatrix}^{-1} \begin{bmatrix} X_3 \\ X_9 \\ X_{15} \\ X_{21} \\ X_{27} \end{bmatrix} \quad (34)$$

The results provide theoretical values to verify WEC-Sim, ensuring proper implementation. The time-domain corollary of Eqs. (32) and (33) is given by the following coupled equations of motion:

$$\begin{aligned} & (m_1 + \mu_{33}(\infty))\ddot{\zeta}_3(t) + \mu_{39}(\infty)\ddot{\zeta}_9(t) + \mu_{315}(\infty)\ddot{\zeta}_{15}(t) + \mu_{321}(\infty)\ddot{\zeta}_{21}(t) \\ & + \mu_{327}(\infty)\ddot{\zeta}_{27}(t) + \int_{-\infty}^t K_{r33}(t-\tau)\dot{\zeta}_3(\tau)d\tau + \int_{-\infty}^t K_{r39}(t-\tau)\dot{\zeta}_9(\tau)d\tau \\ & + \int_{-\infty}^t K_{r315}(t-\tau)\dot{\zeta}_{15}(\tau)d\tau + \int_{-\infty}^t K_{r321}(t-\tau)\dot{\zeta}_{21}(\tau)d\tau \\ & + \int_{-\infty}^t K_{r327}(t-\tau)\dot{\zeta}_{27}(\tau)d\tau + B_g \dot{\zeta}_3(t) + C_{33}\zeta_3(t) = f_{e3}(t) \end{aligned} \quad (35)$$

$$\begin{aligned} & \mu_{93}(\infty)\ddot{\zeta}_3(t) + (m_2 + \mu_{99}(\infty))\ddot{\zeta}_9(t) + \mu_{915}(\infty)\ddot{\zeta}_{15}(t) + \mu_{921}(\infty)\ddot{\zeta}_{21}(t) \\ & + \mu_{927}(\infty)\ddot{\zeta}_{27}(t) + \int_{-\infty}^t K_{r93}(t-\tau)\dot{\zeta}_3(\tau)d\tau + \int_{-\infty}^t K_{r99}(t-\tau)\dot{\zeta}_9(\tau)d\tau \\ & + \int_{-\infty}^t K_{r915}(t-\tau)\dot{\zeta}_{15}(\tau)d\tau + \int_{-\infty}^t K_{r921}(t-\tau)\dot{\zeta}_{21}(\tau)d\tau \\ & + \int_{-\infty}^t K_{r927}(t-\tau)\dot{\zeta}_{27}(\tau)d\tau + B_g \dot{\zeta}_9(t) + C_{99}\zeta_9(t) = f_{e9}(t) \end{aligned} \quad (36)$$

which are implemented in WEC-Sim for the first two bodies. The previous equations provide the general form for each of the other three bodies and it can be seen that five convolution integrals need to be solved per each equation. Without use of the state-space approximation, the computational time increases dramatically with each interacting body, especially if other modes of motion, such as surge and pitch, are included.

The comparisons of the frequency-domain solution to the time-domain solution are provided in Fig. 4 - Fig. 6. The magnitude of the heave response amplitude operator, Fig. 4, shows very good agreement between the frequency- and time-domain solutions with very little variation between bodies. The summation of the RAOs across all bodies, Fig. 5, also shows very good agreement and provides a metric to indicate that the power absorption is relatively equal between both methods. The phase of the RAO provided in Fig. 6, has a significant number of oscillations for the outer bodies in the high frequency regime



yet WEC-Sim is still capable of capturing these effects. A comparison between the uncoupled and coupled equations of motion can be found in Fig. 7, which shows that when neglecting coupling effects the absorbed power can be reduced by up to 20% in the most energetic states.

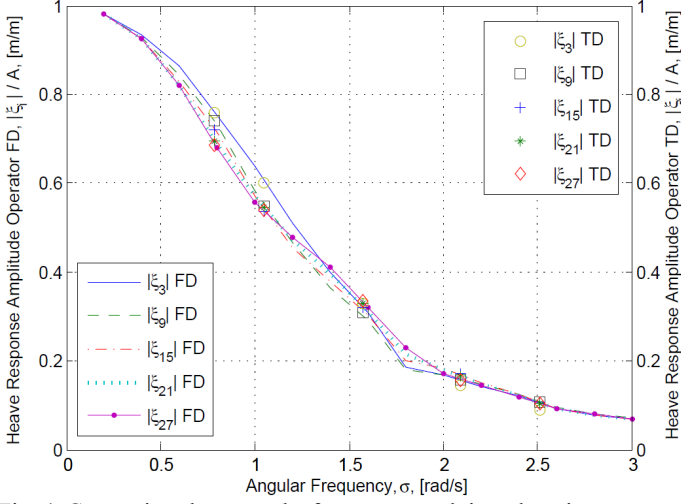


Fig. 4. Comparison between the frequency- and time-domain calculations of the coupled heave motion with  $B_g = 300$  kN/(m/s).

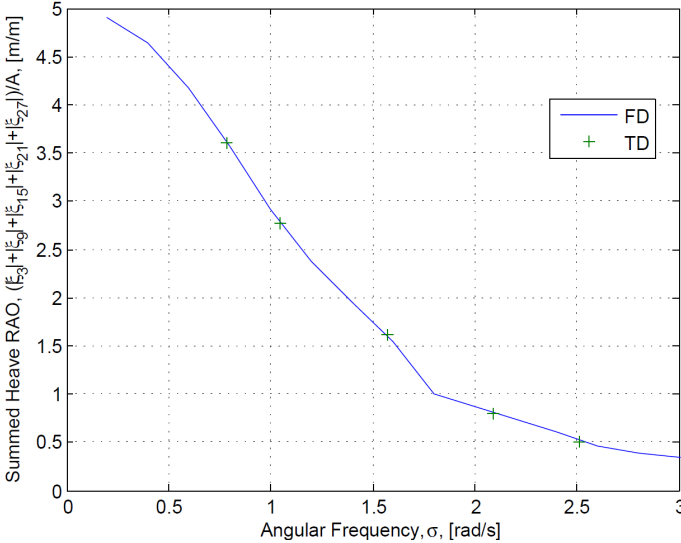


Fig. 5. Comparison of the summed heave motion of the five floating bodies between the frequency- and time-domain coupled calculations.

#### WAVE DIRECTIONALITY, WEATHERVANING, AND USER-DEFINED WAVE ELEVATION

One issue that arises in the design of WECs is the performance sensitivity with respect to wave heading. It can be shown that an asymmetric wave energy converter can have an extraction efficiency up to unity (Madhi, Sinclair, and Yeung, 2013) but the device must be perpendicular to the oncoming wave crest. This may be an appropriate assumption if the device is deployed near shore; however in deep water the device will be subjected to oblique waves likely leading to performance degradation. Furthermore, WECs deployed in deep water will generally rely on mooring lines to provide rotational stiffness thereby allowing the body to yaw where performance again can suffer. Therefore, it is important to have the modeling tools available to allow the WEC to weathervane.

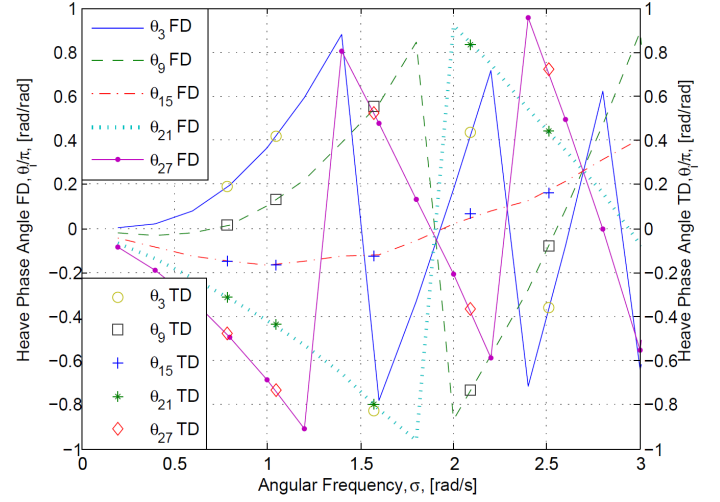


Fig. 6. Comparison of the coupled phase of the five floating bodies between the frequency- and time-domain calculations.

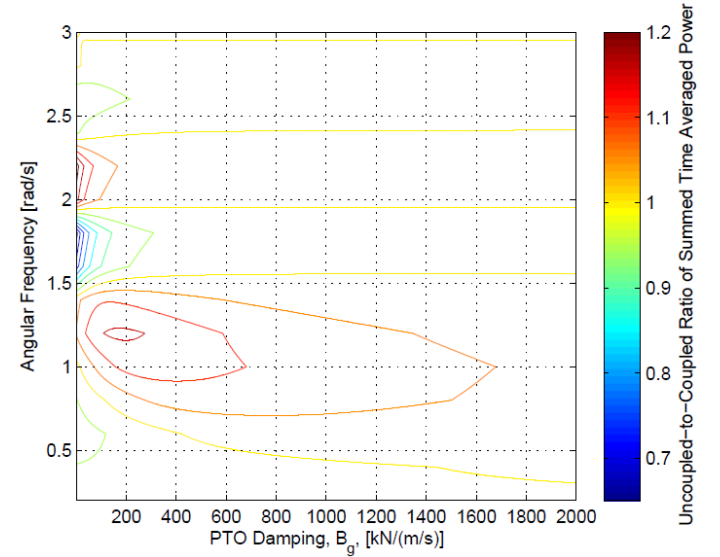


Fig. 7. Ratio of the uncoupled-to-coupled time averaged power.

The incident wave potential,  $\phi_I$ , when accounting for a variable wave heading, is given by:

$$\phi_I(x, y, z, t) = \Re \left\{ \frac{jgA \cosh k(z+h)}{\sigma \cosh kh} e^{j(\sigma - k(x \cos \beta + y \sin \beta))} \right\} \quad (37)$$

where  $g$  is the gravitational acceleration,  $A$  is the wave amplitude,  $k$  is the wave number,  $h$  is the water depth, and  $\beta$  is the wave heading measured counter clockwise from the positive  $x$ -axis. As the wave heading rotates, the only hydrodynamic coefficients that change are the exciting forces because the radiation forces are strictly body-motion-dependent. Most boundary-element methods can be set to output the wave exciting forces for a given number of incident wave angles. However, when the body is free to rotate, the incident wave angle becomes the difference between the wave heading and the yaw angle of the body. Following WAMIT notation,  $\beta$  ranges from 0–360 degrees and a  $2\pi$  correction must be made if the yaw angle exceeds the wave heading as follows:



$$\alpha = \begin{cases} \beta - \xi_6 & \text{if } \xi_6 < \beta \\ 2\pi + \beta - \xi_6 & \text{if } \xi_6 > \beta \end{cases} \quad (38)$$

where  $\alpha$  is the incident wave angle and  $\xi_6$  is the yaw angle of the body measured counter clockwise from the positive x-axis.

For demonstration purposes, a horizontal half cylinder with a radius,  $r$ , of 1 m and a length,  $L$ , of 10 m was chosen as the frontal area changes with wave heading. The half cylinder is assumed to have a uniform density equal to the fluid density. The half cylinder was initially set along the y-axis and was impinged upon by a regular wave with a heading of 22.5 degrees, amplitude of 1 m, and period,  $T$ , of 10 s. A wave-ramp duration equal to five times the wave period was implemented to reduce any impulse effects. The body motion was restricted only to yaw and no external springs were included for yaw stiffness. The results from the simulation can be seen in Fig. 8 and Fig. 9, which depict the body yaw and wave-exciting force time history, respectively. Because the dynamic model is linear, the yaw time history exhibits the typical response of a damped second order system with a constant set point. The body yaws from its initial position overshooting the wave heading before dropping into a decaying oscillation. The overshoot is caused by the system being underdamped despite the addition of a nonlinear drag term. As seen in Fig. 9, the yaw wave-exciting force drops to zero as the yaw angle crosses the heading with smaller oscillations associated with the wave period. In this sense, the exciting force acts as a restoring coefficient based on the difference between yaw angle and wave heading.

Often during tank or sea trials, custom time series are measured and can be imported into WEC-Sim for validation purposes. In order for the user to import a custom wave time series, the excitation force kernel must be constructed. The wave exciting force time series is then obtained by convolving the excitation force kernel with the wave elevation as follows:

$$f_{ei}(t) = \int_{-\infty}^{\infty} K_{ei}(t-\tau)\eta(0,\tau)d\tau. \quad (39)$$

The excitation force kernel is calculated by taking the inverse Fourier transform of the frequency-dependent wave-exciting force coefficients:

$$K_{ei}(t) = \frac{1}{2\pi} \Re \left\{ \int_{-\infty}^{\infty} X_i(\sigma) e^{j\sigma t} d\sigma \right\}. \quad (40)$$

Because  $K_e$  is real, the following identity can be used,  $X_i(-\sigma) = X_i^*(\sigma)$ , where  $*$  in this case denotes the complex conjugate. This simplifies Eq. (40) to:

$$K_{ei}(t) = \frac{1}{\pi} \int_0^{\infty} [\Re\{X_i(\sigma)\} \cos \sigma t - \Im\{X_i(\sigma)\} \sin \sigma t] d\sigma \quad (41)$$

where  $\Re$  and  $\Im$  denote the real and imaginary components, respectively. The half cylinder surge-exciting force kernel is plotted in Fig. 10, which is noncausal because of the time history before  $t = 0$ . The high-frequency oscillations are a result of low resolution of  $X_i$  in the high-frequency regime; however, the oscillations are outside of typical wave frequencies and are filtered out after the convolution. Equation (39) produces the same surge-exciting force when compared to linear superposition theory, verifying proper implementation within WEC-Sim.

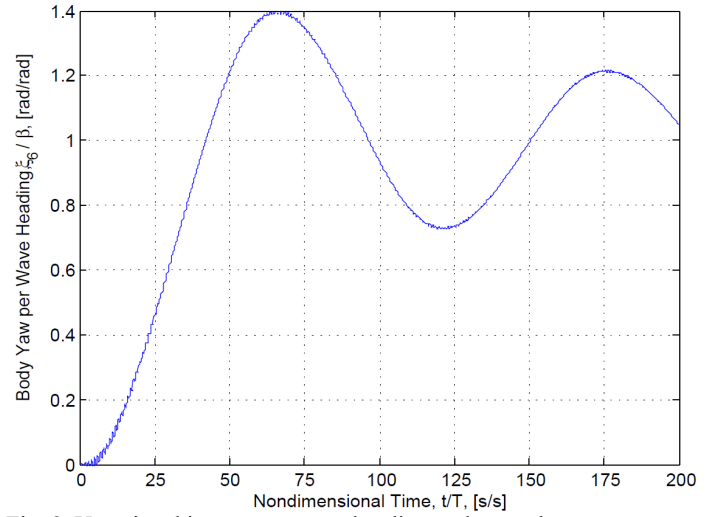


Fig. 8. Yaw time history over wave heading under regular waves.

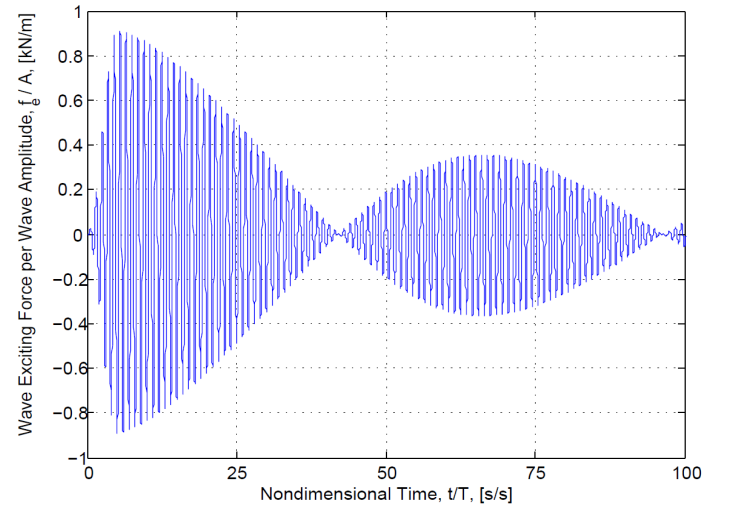


Fig. 9. Yaw-exciting force time history under regular wave excitation.

## CONCLUSIONS

The work presented in this paper highlights several of the new modeling capabilities included in the latest WEC-Sim-v1.1 release. These capabilities include conversion of the fluid memory kernel to state-space form. Simulations showed that over the operating range of frequencies the state-space representation was able to adequately reproduce the hydrodynamic radiation coefficients; however, a relatively high  $R^2$  may need to be set. Because many wave energy converters consist of two or more excited bodies, the ability to model the body-to-body hydrodynamics were added to WEC-Sim. This ability is an important feature to consider during the design process because the effects can lead to reduced floater motion, thereby decreasing annual energy production. Combined with the state-space realization, significant reductions in computational time were observed compared to the default convolution integral calculation. Finally, the hydrodynamic theory allowing a WEC to weathervane and account for wave directionality was presented. Implementation was performed by interpolation of the excitation forces based on the instantaneous incident wave heading. This capability was included because WECs deployed in the open ocean at times will be subject

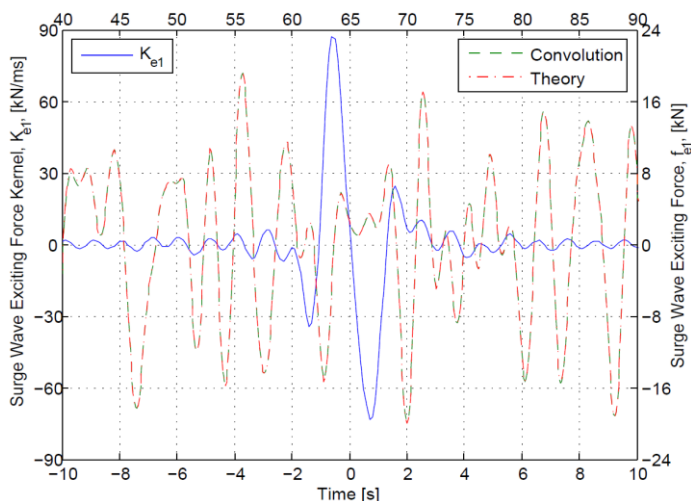


Fig. 10. Surge exciting force kernel for the half cylinder and an irregular surge wave exciting force time history that compares the convolution calculation to the traditional linear superposition theory.

to oblique waves, and the resulting motions and power performance must be evaluated. Furthermore, the theory to calculate the wave-excitation force from a user-defined wave elevation was provided. The test case showed the convolution method provided accurate forces when compared to traditional frequency-based methods; which validates the ability to import custom time series measured during tank tests.

The release of WEC-Sim-v1.1 also includes a module to calculate the instantaneous nonlinear hydrostatic and hydrodynamic forces as described in (Lawson, Yu, Nelessen, Ruehl, and Michelen, 2014). Furthermore, WEC-Sim now boasts the ability to handle Morison elements. However, the fluid particle velocity is calculated assuming the incident wave potential passes undisturbed through the WEC device which is physically unrealistic, but highlights the limitations with mid-fidelity codes. Calculation of the instantaneous fluid velocity and local wave field would require the use of high-fidelity numerical codes that will slow preliminary design iterations. The modeling capabilities of WEC-Sim-v1.1 have significantly increased, and it is now more comparable with other modeling codes. WEC-Sim was developed to assist developers with limited hydrodynamic backgrounds, but as model complexities increase, the user must take additional care in the quality of the hydrodynamic characterization in order to ensure the accuracy of model simulations.

## ACKNOWLEDGMENTS

The authors would like to acknowledge the assistance provided by Kelley Ruehl and Carlos Michelen from Sandia National Laboratories for their assistance in the development of WEC-Sim and the version 1.1 release. This work was supported by the U.S. Department of Energy under Contract No. DE-AC36-08G028308 with the National Renewable Energy Laboratory. Funding for the work was provided by the DOE Office of Energy Efficiency and Renewable Energy, Wind and Water Power Technologies Office.

## REFERENCES

Babarit, A (2014) *NEMOH*, Laboratory for Research in Hydrodynamics, Energy, Environment, and Atmosphere, <http://lhea.ec-nantes.fr/doku.php/emo/nemoh/start?&#nemoh>.

- Combouret, A, Maxime, P, Francois, R., and Barbarit, A (2014). "INWAVE: A New Flexible Design Tool Dedicated to Wave Energy Converters," *Proc. 33rd Intl. Conf. on Ocean, Offshore, and Arctic Eng.*, San Francisco, CA, USA.
- Cummins, WE (1962). "The Impulse Response Function and Ship Motions," *Schiffstechnik*, 9(101).
- Kristiansen, E, Hijulstad, A, and Egeland, O (2005). "State-space Representation of Radiation Forces in Time-domain Vessel Models," *Ocean Eng.*, 32(17–18), 2195–2216.
- Kung, SY (1978). "A New Identification and Model Reduction Algorithm via Singular Value Decompositions," *12th IEEE Asilomar Conf. on Circuits, Systems and Computers*, Pacific Grove, CA, USA, 705–714.
- LaBonte, A, White, B, Lawson, M, Yu, Y-H, Ruehl, K, Bull, D, Li, Y, Thresher, R, Laird, D (2013). "Wave Energy Converter Simulation: Development, Code Competition, and Validation Efforts," *Proc. 10th European Wave and Tidal Energy Conf.*, Aalborg, Denmark, 15.
- Lawson, MJ, Yu, Y-H, Nelessen, A, Ruehl, K, and Michelen, C (2014). "Implementing Nonlinear Buoyancy and Excitation Forces in the WEC-SIM Wave Energy Converter Modeling Tool," *Proc. 33rd Intl. Conf. on Ocean, Offshore, and Arctic Eng.*, San Francisco, CA, USA.
- Lee, CH (1995). *WAMIT Theory Manual*. Massachusetts Institute of Technology.
- Mackay, E, Cruz, J, Livingstone, MJ, and Arnold, P (2013). "Validation of a Time-Domain Modelling Tool for Wave Energy Converter Arrays," *Proc. 10th European Wave and Tidal Energy Conf.*, Aalborg, Denmark, 12.
- Madhi, F, Sinclair, ME, and Yeung, RW (2013). "The "Berkeley Wedge": an Asymmetrical Energy-capturing Floating Breakwater of High Performance," *Marine Sys. Ocean Tech.*, 9(1), 5–16.
- MATLAB Release 2014a, The MathWorks, Inc. (2014). Natick, Massachusetts, United States. Retrieved from <http://www.mathworks.com/products/matlab>.
- Newman, JH (1977). *Marine Hydrodynamics*. Massachusetts Institute of Technology Press, Cambridge, MA.
- Ogilvie, T (1964) "Recent Progress Towards the Understanding and Prediction of Ship Motions," *Proc. 5th Symp. Naval Hydrodynamics*, Washington, D.C., USA, 3-128.
- Orcina, Ltd (2014). *OrcaFlex Manual, Version 9.7a*.
- Perez, T and Fossen TI (2009). "A Matlab Tool for Parametric Identification of Radiation-Force Models of Ships and Offshore Structures," *Modelling, Identification and Control*, 30(1), 1-15.
- Ruehl, K, Michelen, C, Kanner, S, Lawson, M, and Yu, Y-H (2014). "Preliminary Verification and Validation of WEC-Sim, an Open-Source Wave Energy Converter Design Tool," *Proc. 33rd Intl. Conf. on Ocean, Offshore, and Arctic Eng.*, San Francisco, CA, USA.
- Taghipour, E, Perez, T, and Moan, T (2008). "Hybrid Frequency-time Domain Models for Dynamic Response Analysis of Marine Structures," *Ocean Eng.*, 35(7), 685–705.
- Yeung, RW (1981). "Added Mass and Damping of a Vertical Cylinder in Finite-depth Waters," *Appl. Ocean Res.*, 3(3), 119–133.
- Yu, Y-H, Lawson, MJ, Ruehl, K, Michelen, C, and Tom, N (2014). *WEC-Sim on OPENEL*, <http://en.openel.org/wiki/WEC-Sim>.
- Yu, Y-H, Li, Y, Hallet, K, and Hotimsky, C (2014). "Design and Analysis for a Floating Oscillating Surge Wave Energy Converter," *Proc. 33rd Intl. Conf. on Ocean, Offshore, and Arctic Eng.*, San Francisco, CA, USA.
- Yu, Z and Falnes, J (1996). "State-Space Modelling of a Vertical Cylinder in Heave," *Appl. Ocean Res.*, 17(5), 265–275.